Red Blood Cells Initiate Leukocyte Rolling in Postcapillary Expansions: A Lattice Boltzmann Analysis

Chenghai Sun, Cristiano Migliorini, and Lance L. Munn
Department of Radiation Oncology, Massachusetts General Hospital and Harvard Medical School, Boston, Massachusetts

ABSTRACT Leukocyte rolling on the vascular endothelium requires initial contact between leukocytes circulating in the blood and the vessel wall. Although specific adhesion mechanisms are involved in leukocyte-endothelium interactions, adhesion patterns in vivo suggest other rheological mechanisms also play a role. Previous studies have proposed that the abundance of leukocyte rolling in postcapillary venules is due to interactions between red blood cells (RBCs) and leukocytes as they enter postcapillary expansions, but the details of the fluid dynamics have not been elucidated. We have analyzed the interactions of red and white blood cells as they flow from a capillary into a postcapillary venule using a lattice Boltzmann approach. This technique provides the complete solution of the flow field and quantification of the particle-particle forces in a relevant geometry. Our results show that capillary-postcapillary venule diameter ratio, RBC configuration, and RBC shape are critical determinants of the initiation of cell rolling in postcapillary venules. The model predicts that an optimal configuration of the trailing red blood cells is required to drive the white blood cell to the wall.

INTRODUCTION

Initiation of cell rolling is the critical first step in leukocyte adhesion to the vascular endothelium. Both normal and pathological processes such as inflammation, lymph node homing (Warnock et al., 1998), graft rejection, and autoimmune dysfunction rely on leukocyte rolling. Although intense research has characterized the adhesive mechanisms of leukocyte-endothelium interactions, relatively little is known about the mechanical events that cause a cell to *begin* rolling in the vasculature.

Human blood is a concentrated suspension of near-colloidal-size cells in a complex aqueous solution. The red blood cells (RBCs) dominate the cell population on the basis of number and volume concentration. The leukocytes (white blood cells, WBCs) are less easily deformed than red cells and are far fewer in number, with a ratio of about one leukocyte to every 1000 RBCs.

In previous studies, we have shown in vitro (Melder et al., 1995; Munn et al., 1996; Yuan et al., 2001) and in vivo (Melder et al., 2000) that the presence of RBCs greatly enhances leukocyte adhesion to activated endothelium. Mathematical simulations suggest that the mechanism for this involves an increase in leukocyte dispersion and wall contact frequency (Migliorini et al., 2002; Munn et al., 1996). Once rolling is achieved, the RBCs near the plasma rich zone also encourage the continued rolling of the leukocyte, adding a normal force component and torque (Migliorini et al., 2002). But these previous studies were performed in channels, tubes, and vessels of constant diameter, whereas the diameter of a real vessel changes along its length.

The expansion of a capillary into a postcapillary venule is an important example. It has been shown that leukocytes preferentially roll and adhere in postcapillary venules, and that specific adhesive mechanisms are involved (Asako et al., 1992; Bienvenu and Granger, 1993; Johnston et al., 1996; Ley et al., 1993; oude Egbrink et al., 2002; Tsai et al., 1992). But the fluid dynamics of an RBC suspension at a capillary-postcapillary junction are complex, and may also contribute to the abundance of leukocyte-endothelium interactions in these regions.

In capillaries, white blood cells tend to flow with a lower velocity than red blood cells. This is due to the larger volume of the white blood cells, their spherical shape, and the smaller deformation during flow in narrow blood vessels. As a result, red blood cells often accumulate upstream of a white cell in a capillary in single file, whereas downstream of the white cell, a red-cell depleted region is formed. In an interesting large-scale model system, Schmid-Schönbein and co-workers studied this phenomenon and the resulting particle-fluid dynamics at expansion zones, which represented capillary-postcapillary junctions (Schmid-Schönbein et al., 1980). Their results suggest that when a white cell enters an expansion, the trailing red cells pass the slower white cell and thereby displace it away from the vessel axis toward the wall. This RBC-WBC interaction could potentially be responsible for the initiation of cell rolling in postcapillary venules and the propensity for leukocytes to interact in these regions.

It is likely that the hematocrit and RBC aggregation state are important determinants of cell rolling initiation. Pearson and Lipowsky analyzed the effect of RBC aggregation on leukocyte-endothelium (L-E) interactions in mesenteric postcapillary venules, and found enhanced adhesion with larger aggregates and lower flow rates (Pearson and Lipowsky, 2000). But because of the complex fluid dynamics,

Submitted August 20, 2002, and accepted for publication March 21, 2003.

Address reprint requests to Lance L. Munn, Dept. of Radiation Oncology, Mass. General Hospital, 3409 Bldg. 149, Charlestown, MA 02129. Tel.: 617-726-4085; Fax: 617-726-1962; E-mail: lance@steele.mgh.harvard.edu.

Cristiano Migliorini's present address is Aventis Pharma France, Paris, France.

0006-3495/03/07/208/15 $2.00

rigorous analysis of the particle-particle interactions and the forces involved have not been addressed to date.

In this study, we characterize the interactions and estimate the forces involved as RBCs and WBCs interact in capillaries and in postcapillary expansions. Our results suggest that expansion geometry and RBC organization are critical factors that determine the initiation of rolling in postcapillary venules.

METHODS

Fluid and particle dynamics

The red cells are represented by two-dimensional capsules (rectangles with superimposed half-circles at the ends) or ellipses (Case D2 only), and the white cell is modeled as a disk with ligands distributed around the circumference. The capsules and ellipses are defined to have equivalent areas (see Table 1 for dimensions). A lattice Boltzmann method (LBM) adapted to the analysis of fluid suspensions is used to calculate the unsteady flow field and the particle dynamics. The LBM is a relatively new numerical approach for simulating complex flow and transport phenomena in cases where direct solution of the Navier-Stokes equations is not practical (Chen et al., 1992; Qian et al., 1992). Unlike conventional computational methods based on macroscopic continuum equations, the LBM uses the mesoscopic Boltzmann equation to determine macroscopic fluid dynamics. The LBM is flexible, has broad applicability, and may be straightforwardly adapted for parallel computing. Due to the ease of incorporating complex boundary conditions, it has been successfully applied to multiphase and multicomponent fluids, flows through porous media, and solid particle suspensions (for a review, see Chen and Doolen, 1998).

The lattice Boltzmann method treats fluid flow as packets of fluid particles moving from one node to a neighboring node in nine possible directions (which include the possibility of no-movement; see *lower left corner* of Fig. 1). The fluid particles have the following possible discrete velocities:

$$\mathbf{c}_j = \begin{cases} \mathbf{0}, & j = 0, \\ \left(\cos\frac{(j-1)\pi}{2}, \sin\frac{(j-1)\pi}{2}\right), & j = 1,\ldots,4, \\ \left(\cos\left[\frac{(j-5)\pi}{2} + \frac{\pi}{4}\right], \sin\left[\frac{(j-5)\pi}{2} + \frac{\pi}{4}\right]\right), & j = 5,\ldots,8. \end{cases}$$

The LBM solves a discretized BGK (Bhatnagar et al., 1954) form of the Boltzmann equation for the particle density distribution:

$$f_j(\mathbf{x} + \mathbf{c}_j\Delta t,\, t + \Delta t) = f_j(\mathbf{x},\, t) + \Omega_j \tag{1}$$

$$\Omega_j = \frac{1}{\tau}\left[f_j(\mathbf{x},\, t) - f_j^{eq}(\mathbf{x},\, t)\right],$$

where Ω_j is the BGK collision operator, τ is a relaxation time, $\mathbf{x}$ is the location of the lattice node, $\mathbf{c}_j$ is the particle velocity, and f_j^{eq} is the equilibrium distribution that is determined by the fluid density, ρ, and the momentum, $\rho\mathbf{v}$. For a two-dimensional, 9-speed LB model, f_j^{eq} has the following form (see Aidun et al., 1998):

$$f_0^{eq} = \frac{1}{2}\rho,$$

$$f_j^{eq} = \rho\left[\frac{1}{12} + \frac{1}{3}(\mathbf{c}_j\cdot\mathbf{v}) + \frac{1}{2}(\mathbf{c}_j\cdot\mathbf{v})^2 - \frac{1}{2}\mathbf{v}^2\right] \quad \text{for } j = 1,\ldots,4,$$

$$f_j^{eq} = \rho\left[\frac{1}{24} + \frac{1}{12}(\mathbf{c}_j\cdot\mathbf{v}) + \frac{1}{8}(\mathbf{c}_j\cdot\mathbf{v})^2 + \frac{1}{8}\mathbf{v}^2\right] \quad \text{for } j = 5,\ldots,8.$$

Once the particle density distribution is known, we calculate the fluid density, ρ, and momentum, $\rho\mathbf{v}$, using:

$$\rho = \sum_j m f_j(\mathbf{x},\, t)$$

$$\rho\mathbf{v} = \sum_j m\mathbf{c}_j f_j(\mathbf{x},\, t). \tag{2}$$

TABLE 1 Simulation parameters

Parameter	Definition	Value (reference)
A	Hamaker constant	$1 \sim 5 \times 10^{-21}$ J (Bongrand and Bell, 1984; Israelachvili, 1985)
	RBC length (capsular shape)	8.4 μm (Skalak and Chien, 1987)
	RBC thickness (capsular shape)	1.98 μm (Skalak and Chien, 1987)
	RBC length (elliptical shape)	8.4 μm (Migliorini et al., 2002)
	RBC thickness (elliptical shape)	2.4 μm (Migliorini et al., 2002)
R_c	WBC radius	4.5 μm (Skalak and Chien, 1987)
λ	Equilibrium bond length	20 nm (Chang and Hammer, 1996)
K_f	Forward reaction rate	85 s^{-1} (Chang et al., 2000)
K_{r0}	Reverse reaction rate	1×10^{-2} s^{-1} (Chang and Hammer, 1996)
σ	Spring constant	2×10^{-3} N/m (Chang and Hammer, 1996)
σ^*	Transition state spring constant	1×10^{-3} N/m (Chang and Hammer, 1996)
T	Temperature	310 K (Chang and Hammer, 1996)
ν	Plasma kinematic viscosity	1.2×10^{-6} m^2/s (Skalak and Chien, 1987)
u_L	Inlet velocity	1.0×10^{-3} m/s (Schmid-Schönbein et al., 1980)
ρ_c	WBC density	1070 Kg/m^3 (Skalak and Chien, 1987)
ρ_d	RBC density	1098 Kg/m^3 (Skalak and Chien, 1987)
ρ_f	Fluid density	1000 Kg/m^3 (Skalak and Chien, 1987)
H_c	Critical height	40×10^{-9} m (Chang et al., 2000)
D_c	Capillary diameter	10.2×10^{-6} m (Skalak and Chien, 1987)
D_p	Postcapillary diameter	$22.8 \sim 26.4 \times 10^{-6}$ m (Skalak and Chien, 1987)
R_e	Reynolds number ($u_L D_c/\nu$)	8.5×10^{-3} (Chapman and Cokelet, 1997)
N_L	Ligand density	47/μm^2 (Chang and Hammer, 1996) (600 ligands around the cylinder circumference located every 0.45 μm)

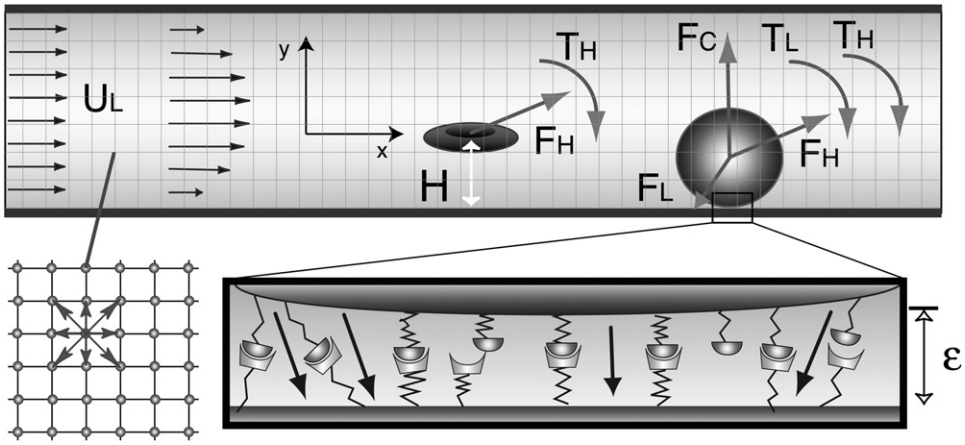

FIGURE 1 A disk representing a leukocyte rolls on the wall of a vessel. The leukocyte interacts with the wall through receptor-ligand interactions and a nonspecific repulsive force. The forces and torques of individual bonds are summed ($\mathbf{F}_L$, T_L) and applied to the leukocyte together with the colloidal ($\mathbf{F}_c$) and hydrodynamic forces and the torque ($\mathbf{F}_H$, T_H). Fluid particle velocities of a two-dimensional lattice Boltzmann model with nine velocities are illustrated at the left lower corner.

It is well-established that with an appropriate equilibrium distribution function and suitable physical limits, the fluid density and velocity obtained using this approach are equivalent to those obtained using the following rigorous Navier-Stokes equations for Newtonian fluids (Bernardin et al., 1991; Qian et al., 1992; Sun, 2000):

$$\frac{\partial \rho}{\partial t} + \nabla \cdot (\rho \mathbf{v}) = 0,$$

$$\rho \frac{\partial \mathbf{v}}{\partial t} + \rho \mathbf{v} \cdot \nabla \mathbf{v} = -\nabla p + \nabla \cdot \{\rho \nu [\nabla \mathbf{v} + (\nabla \mathbf{v})^T]\},$$

where p is the pressure, and ν is the kinematic viscosity. The Navier-Stokes equations are nonlinear partial differential equations which are much more difficult to solve than the discrete, linear equations of the LBM (Eq. 1).

The technique used in the present work for simulating the dynamics of impermeable particle suspensions is based on the approach of Aidun et al. (1998), who modified the original algorithm proposed by Ladd (1994). The method solves the lattice Boltzmann equations on a square lattice with nine directions for the fluid phase (Qian et al., 1992), which is coupled with the Newtonian rotation and translation of solid particles suspended in the fluid through solid-fluid interactions. The cell motion follows Newton's law:

$$\frac{d\mathbf{u}_p}{dt} = \frac{\mathbf{F}}{m_p}; \quad I\frac{d\omega_p}{dt} = T, \tag{3}$$

where $\mathbf{u}_p$ is the velocity of the cell, ω is the angular velocity, T is the torque, I is inertia, and $\mathbf{F}$ is the net force acting on the cell. For RBCs, $\mathbf{F}$ consists only of the hydrodynamic force. For leukocytes, $\mathbf{F}$ includes not only the hydrodynamic force but also the ligand force $\mathbf{F}_L$, and an empirical repulsive van der Waals-like potential interaction $\mathbf{F}_c$ which is defined in Eqs. 5 and 6.

At each iteration, the position of the cell is determined by:

$$\frac{d\mathbf{x}_p}{dt} = \mathbf{u}_p; \quad \frac{d\theta_p}{dt} = \omega_p, \tag{4}$$

where θ_p is the rotational angle of the cell. Equations 3 and 4 are solved using a Runge-Kutta method. The cell's current position and the fluid boundary are then updated.

The repulsive wall interaction is implemented using a Derjaguin approximation (Bongrand and Bell, 1984; Israelachvili, 1985), and prevents the leukocyte from moving into the wall, which would lead to a mathematical singularity. The following force (per unit length) normal to the wall is applied to the center of the leukocyte (Bongrand and Bell, 1984; Israelachvili, 1985):

$$F_c = \frac{A}{8\sqrt{2}}\sqrt{\frac{R_c}{\varepsilon^5}}, \tag{5}$$

where ε is the separation between the surfaces and A is the Hamaker constant. This repulsive van der Waals-like potential exhibits the same behavior as more rigorous expressions that include steric and electrostatic forces (Bongrand and Bell, 1984).

Receptor-ligand model for leukocyte rolling

If the leukocyte approaches within 40 nm of the vessel wall, it can be influenced by stochastic interactions of receptors distributed on the leukocyte with ligands on the wall (Migliorini et al., 2002; see also Fig. 1, this article). The endothelium is assumed to contain a high density of receptor molecules and is uniformly reactive (Bell, 1978; Chang and Hammer, 1996). We use an adhesive dynamics model to describe cell attachment, rolling, and firm adhesion in flow (Hammer and Apte, 1992), which has also been used in similar form by other groups to describe cell-surface interactions (Chang and Hammer, 1996; Dong et al., 1999; Zao et al., 2001). The receptor-ligand bonds are modeled as springs, which provide a force along the bond direction given by:

$$F_L = \sigma(L - \lambda), \tag{6}$$

where L is the bond length, λ is the equilibrium bond length, and σ is the spring constant. The forces contributed by individual ligand-receptor bonds are summed to determine the total bond force and the torque acting on the cell during the period Δt.

If the receptor-ligand distance Y_l is less than a critical value H_c (40 nm), a new bond can form with finite probability P_f (Chang et al., 2000; Dong et al., 1999):

$$P_f = 1 - \exp(-k_{on}\Delta t), \quad Y_l \le H_c, \tag{7}$$

where $k_{on} = k_f N_L$, k_f is the forward reaction rate and N_L is the ligand density.

A preexisting bond is broken with probability P_r, which increases with its current load:

$$P_r = 1 - \exp(-k_r \Delta t); \quad k_r = k_{r0}\exp\left(\frac{(\sigma - \sigma^*)(L-\lambda)^2}{2k_b T}\right), \tag{8}$$

where k_b is the Boltzmann constant, T is the temperature, k_{r0} is the reverse reaction rate, and σ^* is the transition state spring constant.

The procedure for updating the status of receptor-ligand bonds is as follows: the bond status at time t is checked first for each receptor on the WBC. If the receptor is bound to a ligand on the wall at time t, a random number is generated between 0 and 1. If the random number is inferior to P_r determined by Eq. 8, the receptor will disengage at the next time step; otherwise, it will remain bound. If the receptor is free at time t and the

receptor distance from the wall is inferior to H_c, a random number is also generated between 0 and 1. If the random number is inferior to P_f determined by Eq. 7, the receptor will bind to a ligand on the wall at the next time step. Otherwise, it will remain free.

The receptor density correctly influences initial attachment and rolling behavior. For example, increasing the receptor density in Case B2 (described in the Results section) by a factor 4 decreases the rolling velocity by 5.4%. When the receptor density is increased by a factor 10, the rolling velocity decreases dramatically and the WBC actually stops, forming firm adhesion. On the other hand, when the receptor density is decreased by a factor 4 or 10, the rolling velocity increases 7.3% and 9.8%, respectively. But because the current study does not directly address the rolling behavior of the cells after initial attachment, all simulations were performed using a highly reactive surface typical in inflammation to focus on the initial step of rolling.

RESULTS

Capillary flow

Experiments have shown that the most common orientation for red cells to enter a capillary is edge-on, with the axis of symmetry of the cell perpendicular to the axis of the cylinder (Fung, 1984). In vessels with diameter <15 μm, red cells may travel either in single- or multifile, influenced by vessel diameter and tube hematocrit (Skalak and Chien, 1987). In capillaries smaller than the diameter of a RBC, red cells tend to deform in parachute-like shapes and travel in single file groups (Skalak and Brånemark, 1969; Tsukada et al., 2001). As capillary diameter increases, they prefer to travel stacked in multifile (at sufficiently high hematocrit). We first simulated this well-defined case as a test of the model and to provide the initial condition for cells exiting the capillary and entering the postcapillary venule. These simulations were performed for capillaries of 10.2 μm in diameter with three RBCs after a WBC. Because the leukocyte does not contact the wall, no receptor-ligand binding occurs in the capillaries of our simulations.

Case A: leukocyte with three RBCs in a capillary of diameter 10.2 μm

Calculations were carried out using a 600×34 lattice grid corresponding to 180 μm $\times$ 10.2 μm. The computational domain was folded in the x-direction using a uniform velocity profile $\mu_L = 1$ mm/s as the inlet boundary condition and a stress-free condition at the tube outlet (Aidun et al., 1998). In essence, the inlet and outlet are at the same location, which remains 250 grids upstream of the cells. With this folded domain technique we can simulate flow in a very long tube using a relatively small number of lattice nodes in the x-direction. The lattice Boltzmann relaxation time τ was 1, corresponding to a time step of 1.25×10^{-8} s. Initially, a leukocyte and three red cells move in the capillary with velocity μ_L. The red cells enter the center of the capillary with edge-on orientation. The white cell is one grid-point off-center. The simulation corresponds to an actual time interval of 0.45 s, which is normalized to 1 in the figures.

Fig. 2 shows the initial position of the cells before flow commences and snapshots at normalized time $t = 0.111$, 0.222, 0.333, 0.667, and 1.0 (note that the x-axis range increases with time). The velocity distribution (*represented by small arrows*) is parabolic except when disturbed by the cells. As expected from experimental observations, red blood cells flow with a higher velocity than the leukocyte and accumulate upstream of the leukocyte. From $t = 0.333$ until the end of the simulation, the red cells maintain a stacked, single file orientation behind the leukocyte. Because it is

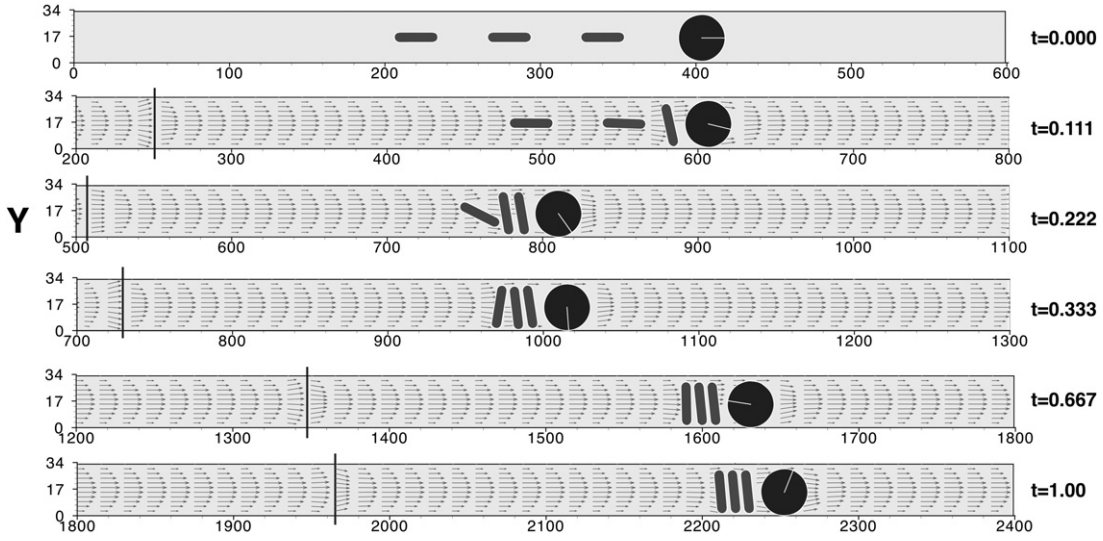

FIGURE 2 Case A. Motion of a leukocyte and three RBCs in a 10.2-μm diameter capillary. Lattice: 600×34. One grid-point unit is equal to 0.3 μm. Total time of 0.45 s is normalized to 1. Velocity field and cell positions at normalized time $t = 0.0$, 0.111, 0.222, 0.333, 0.667, and 1.0. The computational domain was folded in the x-direction, with the inlet and outlet representing the same location (*marked by the vertical bars*), which remains 250 grids upstream of the cells. Note that the x-axis shifts to the right as time increases.

slightly below the tube axis, the white cell rotates with a small angular velocity.

It is interesting that with larger tube diameters and more RBCs, the RBCs did not adopt this stacked arrangement: only the leading two or three RBCs stack behind the WBC, and the rest tumble sequentially behind the WBC (data not shown). Thus, small capillaries appear to be necessary to produce stable RBC stacking.

Simulations at expansions

We next performed three sets of simulations (Cases B, C, and D) to demonstrate the effect of RBCs on WBC margination at the expansion of a tube with a sudden change in diameter from 10.2 μm to 22.8 μm (*Case B*), to 24.6 μm (*Case C*), and to 26.4 μm (*Case D*), respectively.

The inlet geometry and boundary conditions were the same as in Case A. The Reynolds number was 8.5×10^{-3}, and the lattice Boltzmann relaxation time τ was 1, corresponding to a time step of 1.25×10^{-8} s. The simulations correspond to 0.45 s in real time, which was normalized to 1 in the figures. The forces and the torques acting on the WBC were calculated for a cell of 9 μm diameter.

As in the previous case, the WBC starts the simulation one grid-point below center. If the WBC and RBCs are all initially centered about the tube axis, the RBCs catch up with, but never pass, the WBC. They travel down the tube in-line in a persistent, yet unstable configuration. This is because of the ideal geometry of the numerical simulation, which does not allow for small perturbations in trajectory that would upset the unstable configuration and allow the faster RBCs to pass. In a real vessel, the deformability of the cells and the nonsmooth nature of the wall would undoubtedly lead to small fluctuations in the trajectories, thus justifying our initial placement of the WBC slightly off-center.

Case B: expansion from 10.2 μm to 22.8 μm

Cases B1–B2 were carried out using an 800×76 lattice grid corresponding to 240 μm $\times$ 22.8 μm. The vessel has a diameter of 34 grid-points (10.2 μm) at the inlet and expands to a diameter of 76 grid-points (22.8 μm) at $x = 150$ grid. In Case B1, we examine a WBC with no RBCs. In Case B2, three RBCs trail the WBC.

Case B1, leukocyte in the absence of RBCs

Fig. 3 *a* shows snapshots of the WBC at normalized time $t =$ 0, 0.056, 0.333, 0.5, and 0.667. Due to continuity, the plasma disperses as the cross section increases, resulting in a decrease in axial velocity. Driven by hydrodynamic forces, the WBC decelerates and moves slightly downward as it enters the expansion and the velocity profile expands to fill the larger tube. After the initial deviation resulting from the relaxation of the flow field, the net force is essentially zero (Fig. 3, *b–d*), and the leukocyte moves along a straight path, in agreement with experiment (Schmid-Schönbein et al., 1980). Figs. 3, *e–g*, show the resulting *x*-, *y*-, and angular velocities.

Case B2, leukocyte with three RBCs

In this case, the WBC starts at the same position as in Case B1, but with three trailing RBCs. Fig. 4 *a* shows snapshots at normalized time $t = 0$, 0.056, 0.333, 0.5, 0.667, and 0.944. Driven by the hydrodynamic force induced by the RBCs, the leukocyte is forced closer to the bottom wall as it enters the expansion of the vessel (compared to Case B1). The force contributed by the RBCs passing over the WBC is sufficient to cause contact between the WBC and the wall and engagement of receptor-ligand bonds. The WBC rolls slowly along the wall as the transient receptor-ligand bonds resist the hydrodynamic force.

An analysis of the forces shows that that the *x*-velocity of the leukocyte (Fig. 4 *e*) decreases rapidly due to the expansion, and the cell is quickly accelerated toward the wall due to the RBC-influenced hydrodynamic forces (Fig. 4, *c* and *f*). The leukocyte is pushed forward and further downward by this impact. At $t = 0.52$ the leukocyte contacts the wall and ligand-receptor bonds form, causing a negative spike in the net force (Fig. 4 *b*) which results in a sharp deceleration and slowing of the cell (Fig. 4 *e*). As the leukocyte slows down, the hydrodynamic force increases to balance the ligand force and the net force returns to approximately zero (Fig. 4 *b*). Then the leukocyte rolls along the wall at an initial speed of $\sim$160 μm/s which slows to $\sim$142 μm/s after all the RBCs have passed (Fig. 4 *e*). Upon attachment, the angular velocity of the leukocyte increases (Fig. 4 *g*); the negative value corresponds to clockwise rotation. The oscillations in force and velocity after attachment are due to stochastic formation and dissociation of individual receptor-ligand bonds.

The next set of simulations shows that if the expansion diameter is increased, three RBCs are not sufficient to initiate WBC rolling.

Case C: expansion from 10.2 μm to 24.6 μm

Now we increase the expansion diameter by six grids. Cases C1–C3 were performed using an 800×82 lattice grid corresponding to 240 μm $\times$ 24.6 μm. The vessel has a diameter of 34 grid-points (10.2 μm) at the inlet and expands to a diameter of 82 grid-points (24.6 μm) at $x = 150$ grid. We follow one WBC with three, four, and five RBCs in Cases C1, C2, and C3, respectively.

Case C1, leukocyte with three RBCs

The initial cell configuration is the same as Case B2, i.e., the leukocyte is initially one grid-point off-center toward the

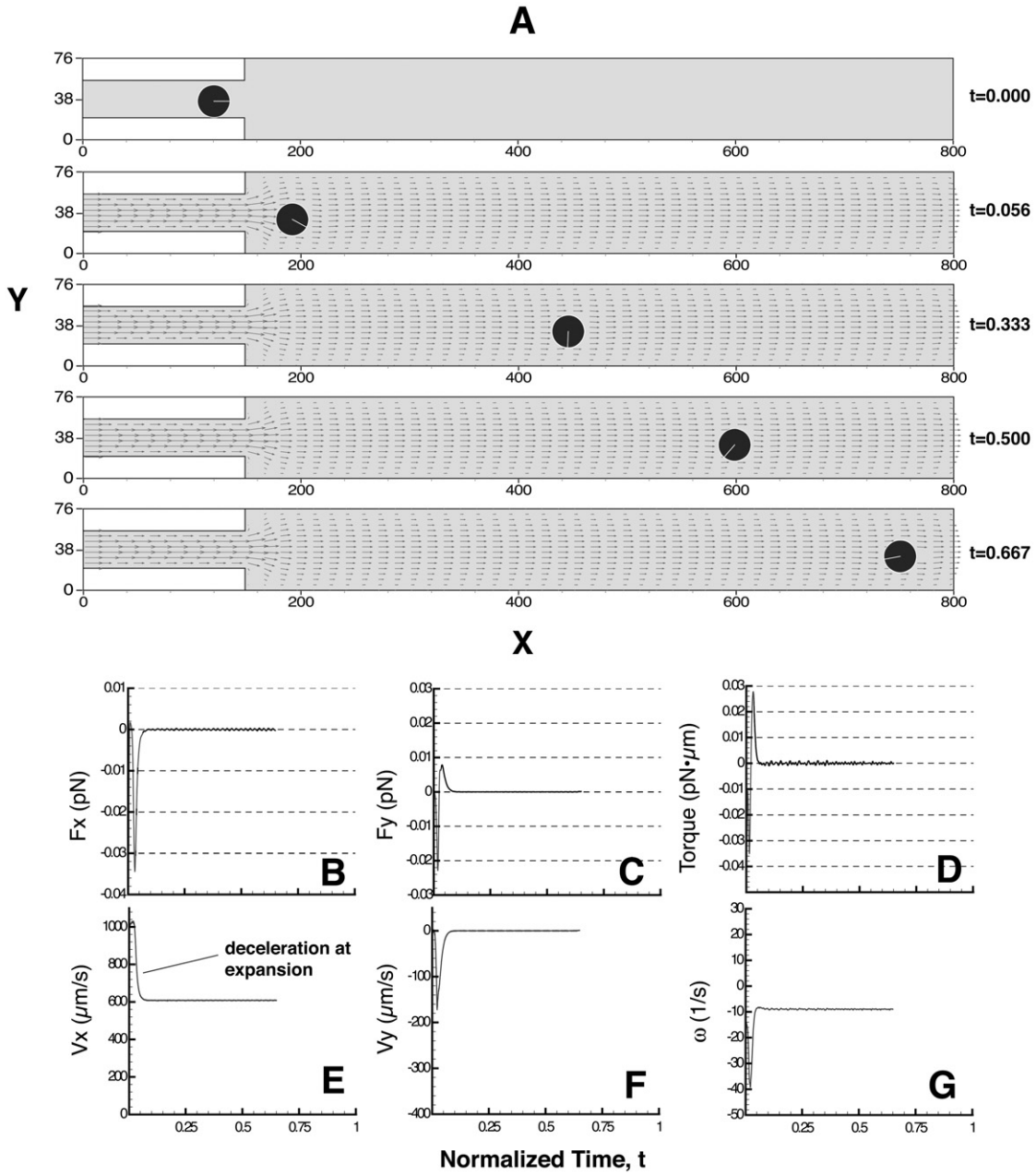

FIGURE 3 Case B1. Leukocyte motion in the absence of RBCs (small expansion). Lattice: 800 × 76. One grid-point unit is equal to 0.3 μm. Total time of 0.45 s is normalized to 1. (*a*) Velocity field and cell positions at normalized time $t = 0$, 0.0556, 0.333, 0.5, and 0.667. (*b–g*) net *x*-force (F_x), net *y*-force (F_y), torque, *x*-velocity (V_x), *y*-velocity (V_y), and angular velocity (ω) versus normalized time.

bottom wall and the RBCs are at the center. However, the expansion diameter is larger than that of Case B2.

Fig. 5 *a* shows snapshots at normalized time $t = 0$, 0.056, 0.333, 0.5, 0.667, and 0.944. Similar to the two preceding cases, the leukocyte slows and moves downward as it enters the expansion. The hydrodynamic force induced by the RBCs pushes the leukocyte closer to the bottom wall as it enters the expansion of the vessel. Its radial movement is further increased as the three RBCs pass over the leukocyte. However, in this case, the WBC does not come close enough to the wall (i.e., <40 nm) to engage receptor-ligand binding because of the larger expansion. Fig. 5, *b–g* presents the net forces and torque acting on the leukocyte and its velocity components.

Case C2, leukocyte with four RBCs

In this case we add one more RBC to Case C1 to investigate whether an increase in the number of RBCs affects the WBC movement.

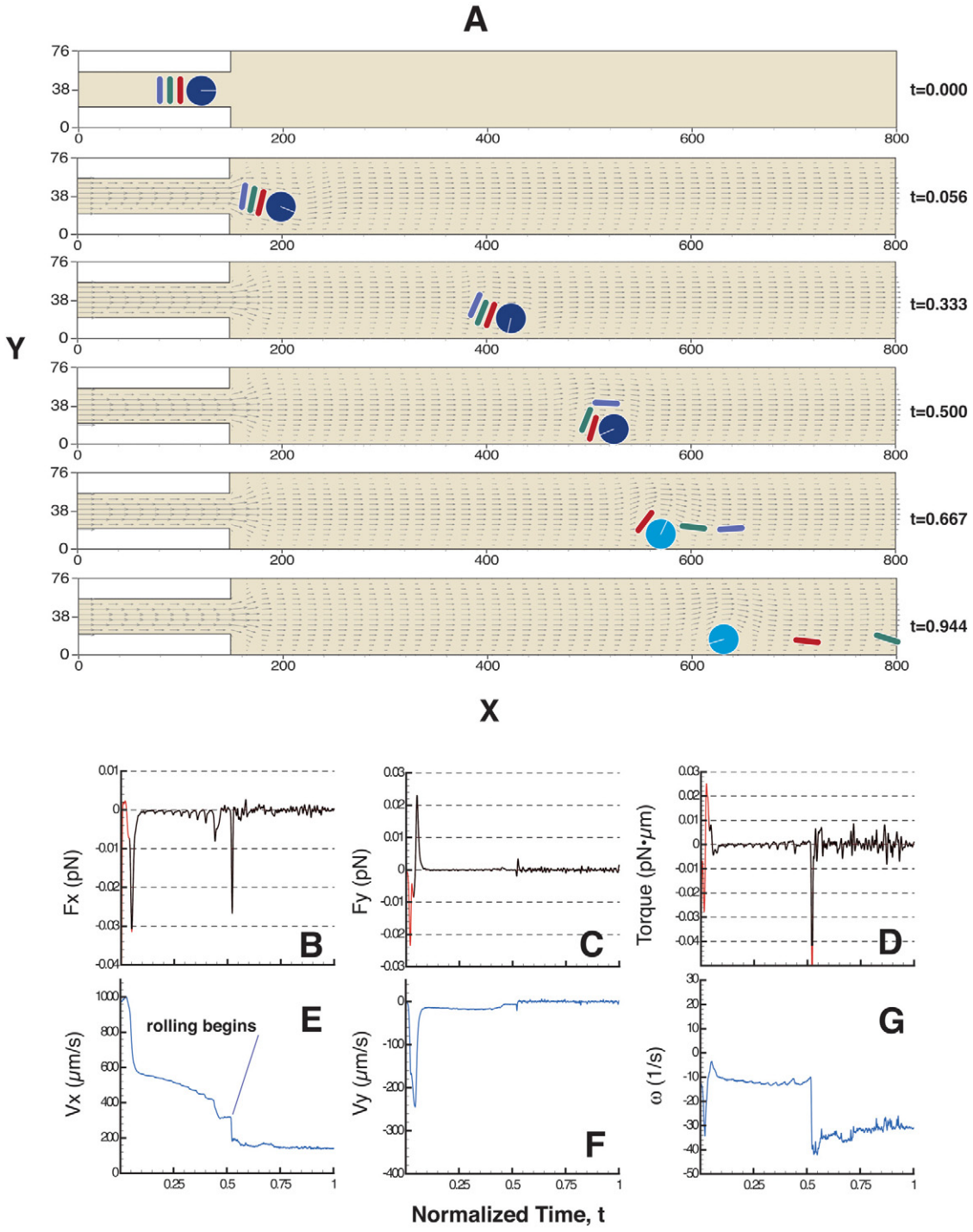

FIGURE 4 Case B2. Leukocyte motion with three RBCs (small expansion). Lattice: 800 × 76. One grid-point unit is equal to 0.3 μm. Total time of 0.45 s is normalized to 1. (*a*) Velocity field and cell positions at normalized time $t = 0$, 0.056, 0.333, 0.5, 0.667, and 0.944. Red blood cells are represented by different colors for tracking purposes; lighter shading of the WBC indicates rolling on the wall. (*b–g*) net *x*-force (F_x), net *y*-force (F_y), torque, *x*-velocity (V_x), *y*-velocity (V_y), and angular velocity (ω) versus normalized time. At $t = 0.52$ the leukocyte contacts the wall and ligand-receptor bonds form.

Fig. 6 *a* shows snapshots at normalized time $t = 0$, 0.056, 0.333, 0.5, 0.667, and 0.944. Compared to Case C1, the additional RBC passing over the WBC provides sufficient force to push the WBC close enough to the wall for ligand bond to engage at $\sim t = 0.5$. The WBC then begins rolling and slows down. The force and velocity profiles of the WBC plotted in Fig. 6, *b–g*, are similar to those of Case B2, which has one fewer RBC and a smaller expansion diameter. Since the flow rate is the same in all cases, the larger postcapillary diameter has

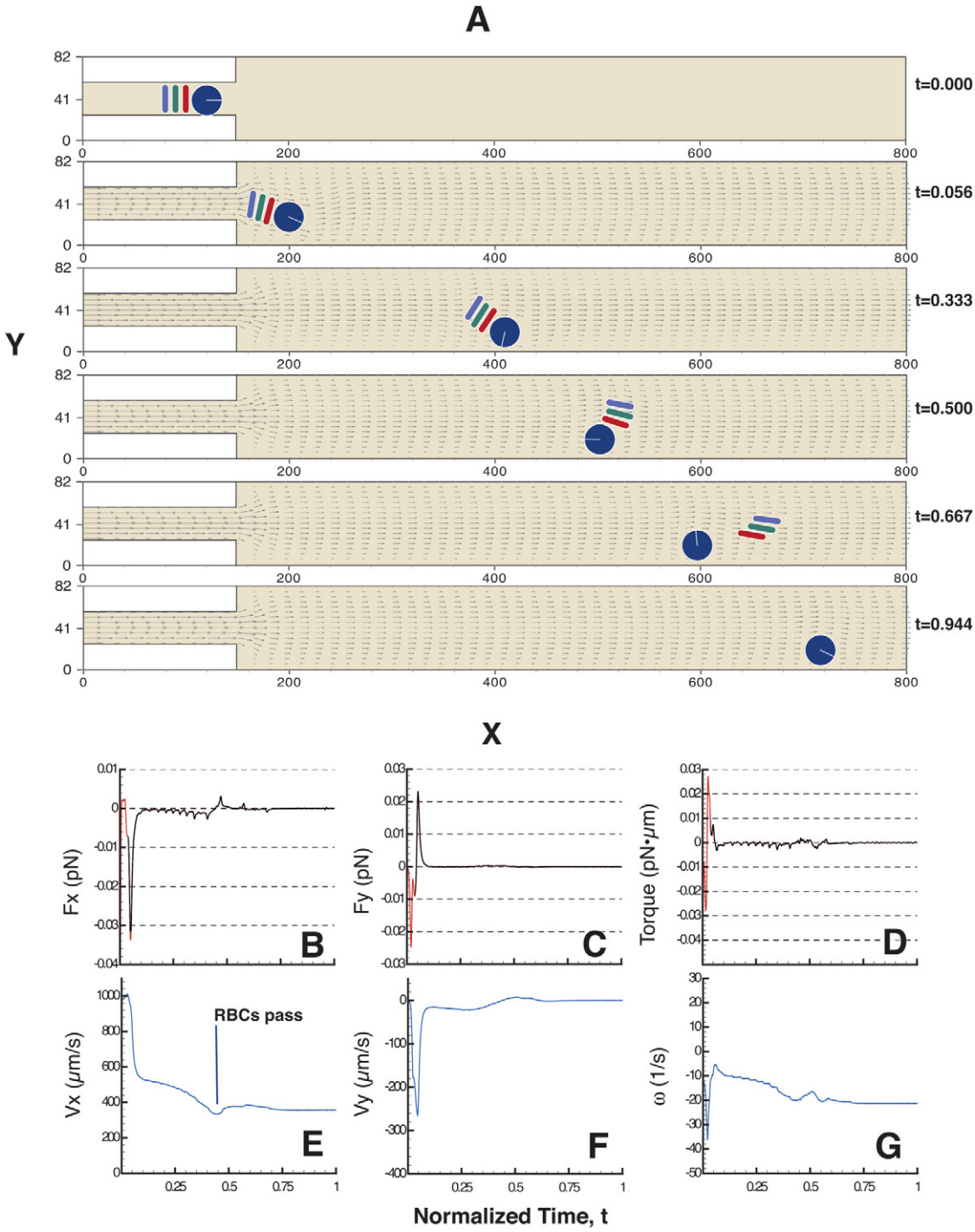

FIGURE 5 Case C1. Leukocyte motion with three RBCs (intermediate expansion). Lattice: 800 × 82. One grid-point unit is equal to 0.3 μm. Total time of 0.45 s is normalized to 1. (*a*) Velocity field and cell positions at normalized time $t = 0$, 0.056, 0.333, 0.5, 0.667, and 0.944. Red blood cells are represented by different colors for tracking purposes. (*b–g*) net *x*-force (F_x), net *y*-force (F_y), torque, *x*-velocity (V_x), *y*-velocity (V_y), and angular velocity (ω) versus normalized time. The WBC does not come close enough to the wall to initiate adhesion.

a lower shear rate (see Table 2). Because of this decrease in shear rate, the rolling velocity drops to 116 μm/s from 142 μm/s (see Fig. 6 *e*) when the postcapillary diameter increases to 24.6 μm from 22.8 μm.

Case C3, leukocyte with five RBCs

In this case we add another RBC to Case C2. Fig. 7 *a* shows snapshots at normalized time $t = 0$, 0.056, 0.333, 0.5, 0.667,

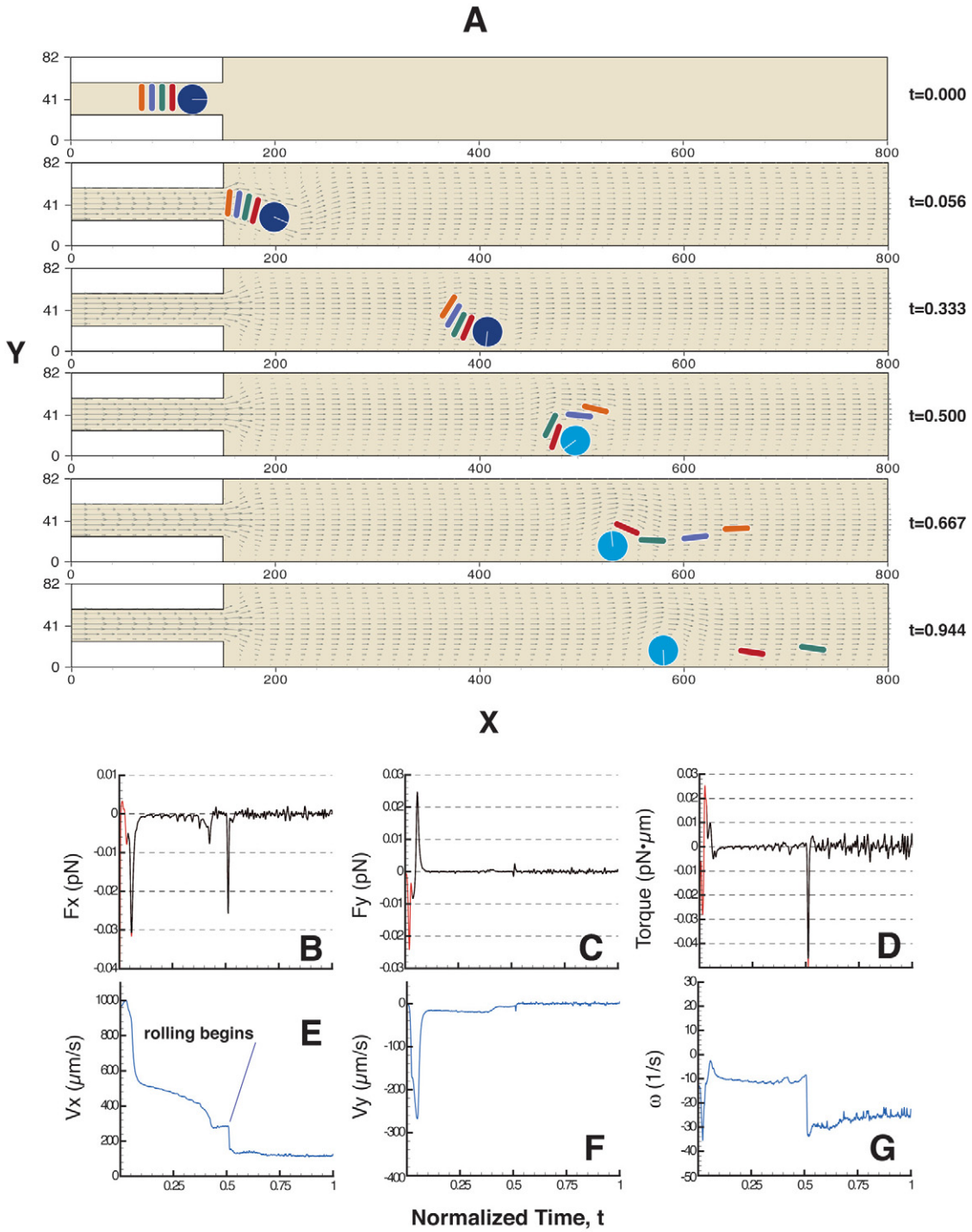

FIGURE 6 Case C2. Leukocyte motion with four RBCs (intermediate expansion). Lattice: 800 × 82. One grid-point unit is equal to 0.3 μm. 0.45 s is normalized to 1. (*a*) Velocity field and cell positions at normalized time $t = 0$, 0.056, 0.333, 0.5, 0.667, and 0.944. Red blood cells are represented by different colors for tracking purposes; lighter shading of the WBC indicates rolling on the wall. (*b–g*) net *x*-force (F_x), net *y*-force (F_y), torque, *x*-velocity (V_x), *y*-velocity (V_y), and angular velocity (ω) versus normalized time. Receptor-ligand binding occurs at $t = 0.5$.

and 0.944. It is interesting that when a rouleau of RBCs this large exits the capillary (see Fig. 7 *a* at $t = 0.056$) there are recirculation zones in the upper and lower corners that disappear as the cells move away from the capillary. Fig. 7, *b–g*, present the net forces and torque acting on the leukocyte and its velocity components. Because the tube is not large enough, the 5-RBC rouleau becomes disrupted before it passes the WBC. The two leading RBCs are pushed downward by the others and are not able to pass the WBC. The force contributed by the RBCs passing over the WBC is

TABLE 2 Summary of simulations

Case	D_p	D_p/D_c	S (1/s)	RBCs	ΔY (μm)	Adhesion?	V_x (μm/s)	V_{roll} (μm/s)	$\Delta V/V_{roll}$
B1 (Fig. 3)	22.8	2.24	118	0	4.80	no	608.3	40.482	1402%
B2 (Fig. 4)	22.8	2.24	118	3	0.0054	yes	141.6	136.97	3.38%
C1 (Fig. 5)	24.6	2.41	101	3	0.858	no	353.3	82.926	326%
C2 (Fig. 6)	24.6	2.41	101	4	0.009	yes	115.8	112.37	3.05%
C3 (Fig. 7)	24.6	2.41	101	5	1.447	no	392.2	90.684	332%
D1 (Fig. 8)	26.4	2.59	87.8	5	0.009	yes	98.28	95.38	3.03%
D2 (Fig. 9)	26.4	2.59	87.8	5	0.1812	no	177.8	71.53	149%

D_p/D_c is the postcapillary:capillary diameter ratio, where the capillary diameter, D_c is 10.2 μm for all cases; D_p is the postcapillary diameter. S is the postcapillary wall shear rate in the developed flow, distant from cell disturbances. ΔY is the minimum separation distance between the WBC and the postcapillary wall. V_x is the x-velocity at the position of closest approach to the wall. V_{roll} is the equivalent rolling velocity calculated as $V_{roll} = R_c{*}\omega$, where R_c is the WBC radius and ω is average angular velocity at closest approach. $\Delta V/V_{roll}$ is the relative difference between V_x and V_{roll}, i.e., $\Delta V/V_{roll}=(V_x - V_{roll})/V_{roll}$. Because of a small amount of slip at the surface, values of $\sim$3% indicate rolling.

not sufficient to cause adhesion of the WBC to the wall. The final x-velocity of the leukocyte is higher than that of Case C1 because it is farther from the wall.

In the next example, we demonstrate that if the expansion diameter is increased further, the same 5-cell rouleau of RBCs can induce WBC rolling.

Case D: expansion from 10.2 μm to 26.4 μm

Here we increase the expansion diameter again by six grids. Cases D1–D2 were performed using an 800×88 lattice grid corresponding to 240 μm $\times$ 26.4 μm. The vessel has a diameter of 34 grid-points (10.2 μm) at the inlet and expands to a diameter of 88 grid-points (26.4 μm) at $x = 150$ grid. We introduce one WBC followed by five RBCs in both Case D1 and Case D2. But in Case D2, the RBCs are ellipsoidal rather than rectangular to investigate the effect of RBC shape.

Case D1, leukocyte with five RBCs

The initial configuration of the WBC and five RBCs and the inlet fluid conditions in the capillary are the same as that of Case C3. The expansion diameter is six grids larger than that of Case C3.

Fig. 8 *a* shows snapshots at normalized time $t = 0$, 0.056, 0.333, 0.5, 0.667, and 0.944. Compared to Case C3, all five RBCs pass over the WBC in this larger expansion and provide sufficient force to push the WBC close enough to the wall for ligand bonds to engage at $\sim t = 0.6$, at which point the WBC decelerates and starts rolling. The force and velocity profiles of the WBC are plotted in Fig. 8, *b–g*. They are similar to those of Cases B2 and C2 in which WBC adhesion took place. Again, because the tube diameter is larger, the rolling velocity is lower, $\sim$98 μm/s (Fig. 8 *e*). This value of rolling velocity is in agreement with experimental studies (Munn et al., 1996).

Case D2, leukocyte with five ellipsoidal RBCs

Since it appears that maintaining the stacked arrangement of RBCs is important in inducing adhesion, we next simulated ellipsoidal RBCs, which are less stable in a stacked configuration. The number of RBCs and the geometry of the vessel are the same as Case D1.

Fig. 9 *a* shows snapshots at normalized time $t = 0$, 0.056, 0.222, 0.333, 0.5, and 0.667. Fig. 9, *b–g*, presents the net forces and torque acting on the leukocyte and its velocity components. Because the train of ellipsoids is less stable than the previous stacks of flat RBCs (such as in Case D1), it tends to bend (see the snapshots at $t = 0.056$ and 0.222) and pushes the WBC to the wall with more force at the beginning. But the train disrupts quickly and the disorganized group of ellipses passes the WBC more easily (compare Figs. 9 *a* and 8 *a* at $t = 0.333$ and 0.5). This results in a lower time of interaction and less influence on the WBC. Therefore, the WBC does not contact the wall although it comes in close proximity (0.18 μm from the wall).

Table 2 summarizes the results from the various simulations. Listed are the expansion diameter, the number of RBCs, the adhesion status, the closest approach distance between WBC and the wall, and the corresponding WBC velocities (V_x) at this position. We also calculated an equivalent rolling velocity ($V_{roll} = R_c{*}\omega$), where R_c is the radius of the WBC and ω is the average angular velocity at the minimum gap. If V_{roll} is equal to V_x, the WBC is rolling (cases B2, C2, and D1). In the other cases, the WBC velocity is much higher than the equivalent rolling velocity.

DISCUSSION

Our results show that initiation of leukocyte rolling in postcapillary venules is a delicate process, sensitive to vessel geometry and the organization of RBCs in the upstream capillary. The geometry chosen for Cases B–D was based on the experiments of Schmid-Schönbein et al. (1980), and represents an ''ideal'' expansion with diameter ratio representative of that found in capillary-postcapillary junctions. It is interesting to speculate that the expansion geometry in vivo is not arbitrary, but has evolved to an optimal configuration that encourages leukocyte attachment.

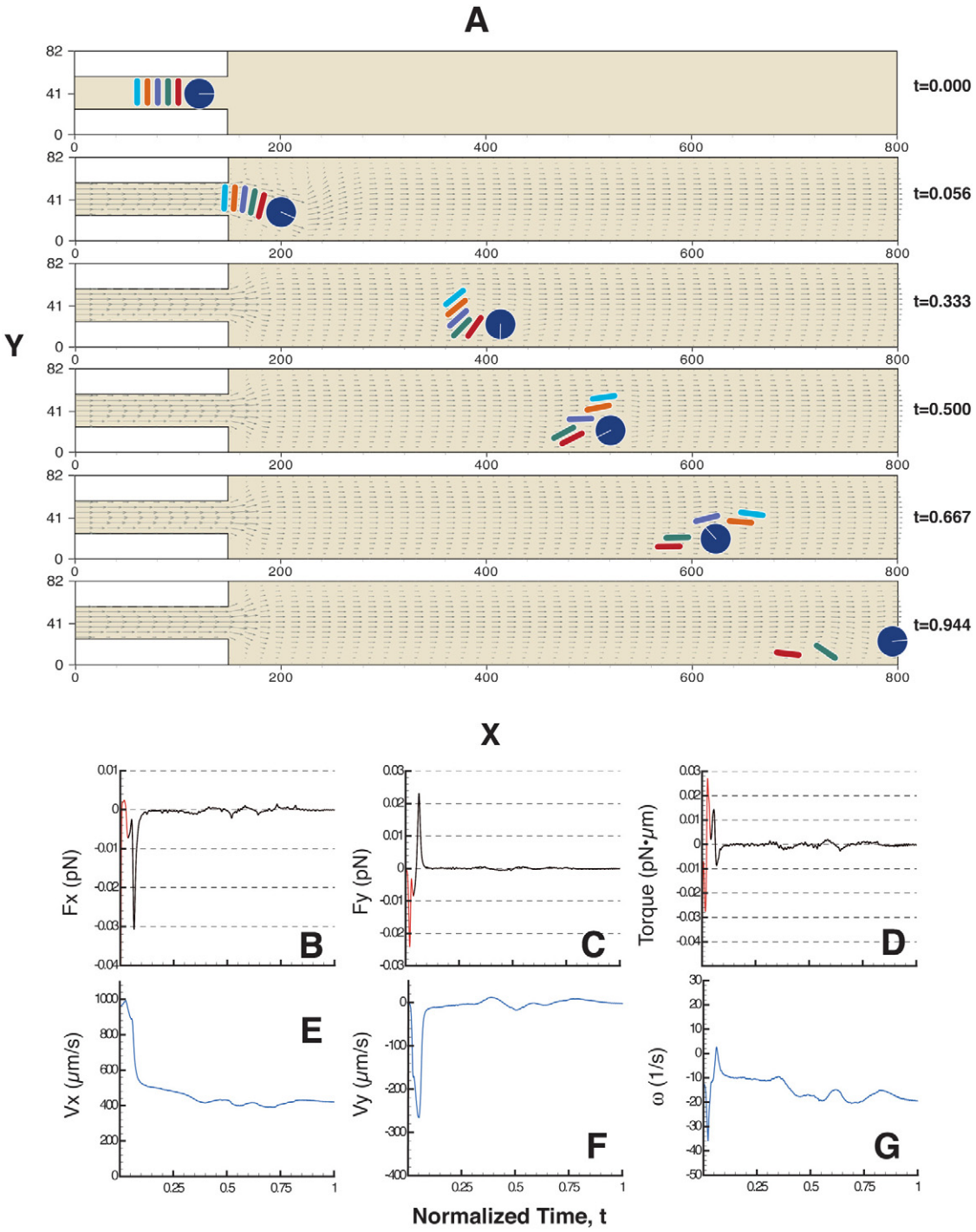

FIGURE 7 Case C3. Leukocyte motion with five RBCs (intermediate expansion). Lattice: 800 × 82. One grid-point unit is equal to 0.3 μm. Total time of 0.45 s is normalized to 1. (*a*) Velocity field and cell positions at normalized time $t = 0.0$, 0.056, 0.33, 0.5, 0.67, and 0.94. Red blood cells are represented by different colors for tracking purposes. (*b–g*) net *x*-force (F_x), net *y*-force (F_y), torque, *x*-velocity (V_x), *y*-velocity (V_y), and angular velocity (ω) versus normalized time. The WBC does not come close enough to the wall to initiate adhesion.

Table 2 summarizes the influence of expansion diameter and the number of RBCs on WBC adhesion. For a given expansion diameter there appears to be an optimal configuration of the trailing RBCs required to drive the WBC to the wall. In our simulations, WBC adhesion occurred in Case B2 (expansion diameter 22.8 μm, three RBCs), Case C2 (expansion diameter 24.6 μm, four RBCs), and Case D1 (expansion diameter 26.4 μm, five RBCs). Thus, larger expansions require more RBCs. But too many RBCs cannot maintain a stacked arrangement, and become disorganized

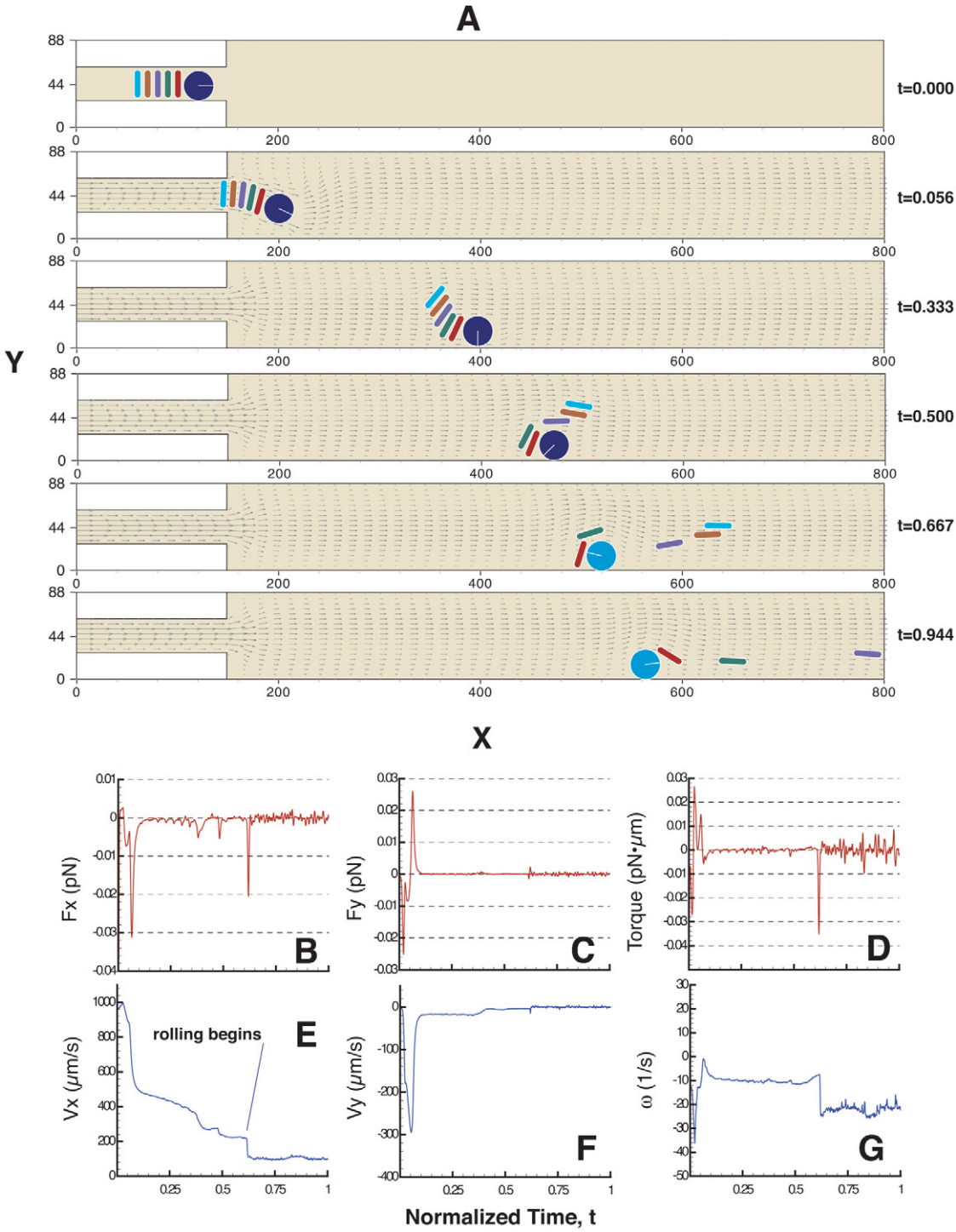

FIGURE 8 Case D1: Leukocyte motion with five RBCs (large expansion). Lattice: 800 × 88. One grid-point unit is equal to 0.3 μm. 0.45 s is normalized to 1. (*a*) Velocity field and cell positions at normalized time $t = 0$, 0.056, 0.333, 0.5, 0.667, and 0.944. Red blood cells are represented by different colors for tracking purposes; lighter shading of the WBC indicates rolling on the wall. (*b–g*) net *x*-force (F_x), net *y*-force (F_y), torque, *x*-velocity (V_x), *y*-velocity (V_y), and angular velocity (ω) versus normalized time. Receptor-ligand binding occurs at $t = 0.6$.

too early before they pass the WBC. Our results show that a coherent rouleau of RBCs is more effective at pushing the WBC to the wall than a loosely-associated group of cells. Previous studies have concluded that RBC aggregation is an important determinant of L-E interactions in postcapillary venules (Mayrovitz et al., 1987; Pearson and Lipowsky, 2000). Although we did not directly address RBC aggregation in the current study, our results suggest that groups

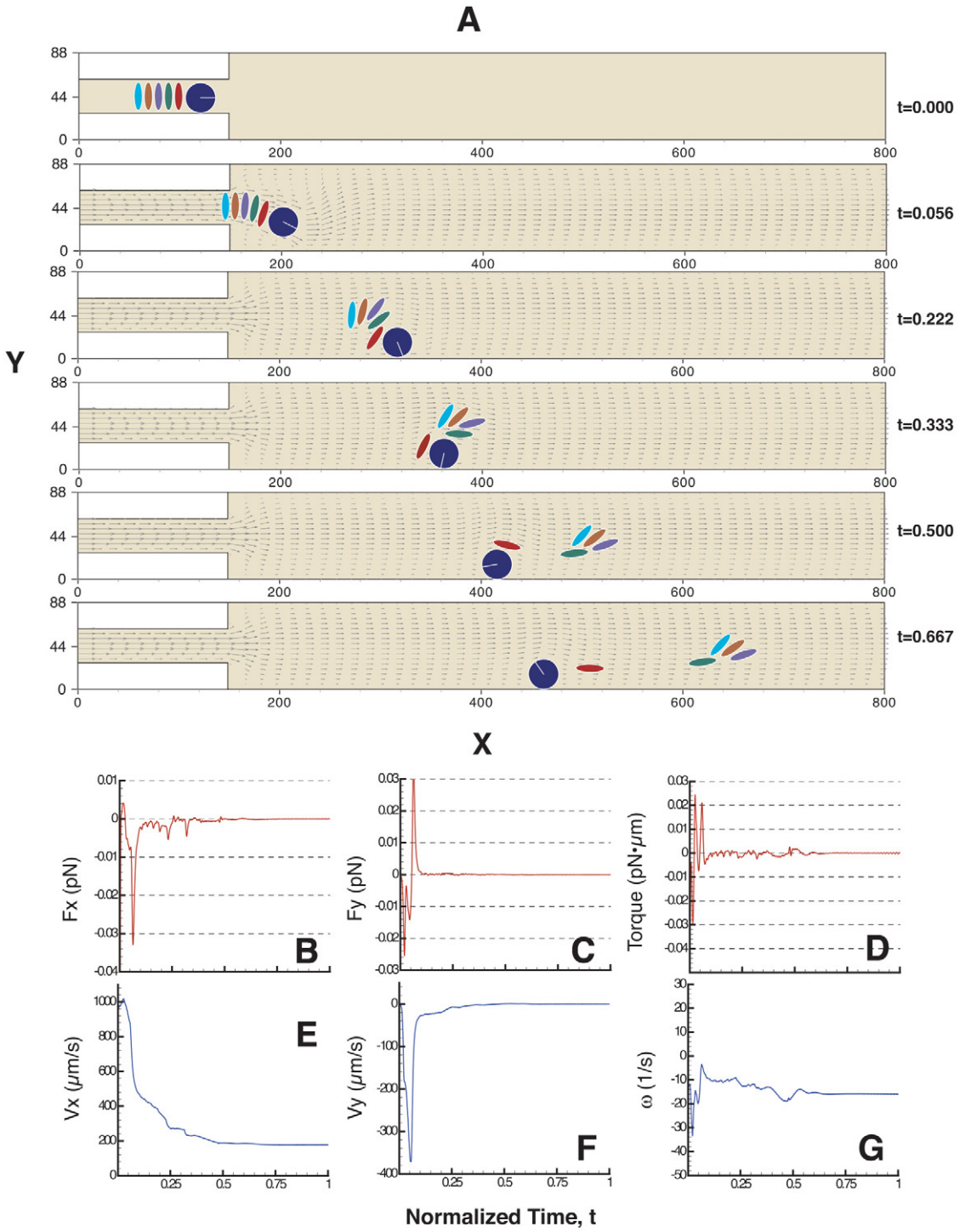

FIGURE 9 Case D2: Leukocyte motion with five ellipses (large expansion). Lattice: 800 × 88. One grid-point unit is equal to 0.3 μm. 0.45 s is normalized to 1. (*a*) Velocity field and cell positions at normalized time $t = 0$, 0.056, 0.222, 0.333, 0.5, and 0.667. Ellipses are represented by different colors for tracking purposes. (*b–g*) net *x*-force (F_x), net *y*-force (F_y), torque, *x*-velocity (V_x), *y*-velocity (V_y), and angular velocity (ω) versus normalized time. The WBC does not come close enough to the wall to initiate adhesion.

consisting of 3–5 RBCs separated by plasma will lead to greater radial motion of the leukocyte. The formation of these groups should depend on the relative numbers of RBCs and WBCs in the blood, the fluid dynamics at the capillary inlet, and the propensity of the RBCs to aggregate.

The shape of the RBCs in our simulations affected their ability to stay in a stacked formation. RBCs are actually biconcave disks, but in profile they appear as rectangles with round ends. As our simulations show, a rouleau of flat RBCs behaves quite differently from a train of ellipses of the same

size. Whereas flattened shapes can easily form rouleaux and therefore provide sufficient force to initiate WBC rolling, the ellipsoidal RBCs tended to ''roll'' against one another, leading to disruption of the initial stacking arrangement.

Another interesting observation is that the blood vessels in solid tumors, as opposed to normal tissues, do not follow the same hierarchical progression from artery to vein. Instead, tumor angiogenesis results in a chaotic, malformed network with no apparent organization (Less et al., 1991). Thus they do not have normal capillary-postcapillary expansions. Tumors are also notoriously proficient at evading immune surveillance by leukocytes. It is possible that this is, at least in part, due to the inability of the leukocytes to initiate rolling within tumor vessels.

CONCLUSIONS

We have, for the first time, estimated the hydrodynamic forces exerted in flowing blood that lead to cell rolling in postcapillary venules. The lattice Boltzmann simulations presented here demonstrate the utility of this technique in analyzing the dynamics of complex particle suspensions such as blood. This first multibody simulation in a relevant geometry provides a better understanding of the mechanism of leukocyte rolling, and shows that expansion geometry, RBC organization, and RBC shape play important roles in the initiation of leukocyte rolling in postcapillary venules. We conclude that, depending on the expansion diameter, there is an optimal configuration of the trailing RBCs required to drive the WBC to the wall. Future studies should further examine the roles of RBC aggregation and deformability in this process.

We acknowledge Dr. R. K. Jain, Dr. Y. H. Qian, Dr. H. Chen, Dr. G. W. Schmid-Schönbein, B. R. Stoll, T. Padera, and Dr. T. Roose for helpful discussions. We are also grateful to Dr. C. K. Aidun and Dr. E. J. Ding for providing their lattice Boltzmann codes, on which this model was based.

This work was supported by National Institutes of Health grant R01 HL64240 (to L.L.M.).

REFERENCES

Aidun, C. K., Y. Lu, and E. J. Ding. 1998. Direct analysis of particulate suspensions with inertia using the discrete Boltzmann equation. *J. Fluid Mech.* 373:287–311.

Asako, H., P. Kubes, B. A. Baethge, R. E. Wolf, and D. N. Granger. 1992. Colchicine and methotrexate reduce leukocyte adherence and emigration in rat mesenteric venules. *Inflammation.* 16:45–56.

Bell, G. I. 1978. Models for the specific adhesion of cells to cells. *Science.* 200:618–627.

Bernardin, D., O. E. Seroguillaume, and C. H. Sun. 1991. Multispecies 2D lattice gas with energy-level-diffusive properties. *Physica D.* 47:169–188.

Bhatnagar, P., E. Gross, and M. Krook. 1954. A Model for collision processes in gases. 1. Small amplitude processes in charged and neutral one-component systems. *Phys. Rev.* 94:511–525.

Bienvenu, K., and D. N. Granger. 1993. Molecular determinants of shear rate-dependent leukocyte adhesion in postcapillary venules. *Am. J. Physiol.* 264:H1504–H1508.

Bongrand, P., and G. I. Bell. 1984. Cell-cell adhesion: parameters and possible mechanisms. *In* Cell Surface Dynamics: Concepts and Models. A. Perelson, C. DeLisi, and F. W. Wiegel, editors. Marcel Dekker, New York.

Chang, K., and D. A. Hammer. 1996. Influence of direction and type of applied force on the detachment of macromolecularly-bound particles from surfaces. *Langmuir.* 12:2271–2282.

Chang, K., D. F. J. Tees, and D. A. Hammer. 2000. The state diagram for cell adhesion under flow. *Proc. Natl. Acad. Sci. USA.* 97:11262–11267.

Chapman, G. B., and G. R. Cokelet. 1997. Model studies of leukocyte-endothelium-blood interaction. *Biorheology.* 34:37–56.

Chen, H., S. Chen, and W. H. Matthaeus. 1992. Lattice Boltzmann model for simulating flows with multiple phases and components. *Phys. Rev. A.* 45:5339–5342.

Chen, S., and G. D. Doolen. 1998. Lattice Boltzmann method for fluid flows. *Annu. Rev. Fluid Mech.* 30:329–364.

Dong, C., J. Cao, E. J. Struble, and H. H. Lipowsky. 1999. Mechanics of leukocyte deformation and adhesion to endothelium in shear flow. *Ann. Biomed. Eng.* 27:298–312.

Fung, Y. C. 1984. Biodynamics: Circulation. Springer-Verlag, New York.

Hammer, D. A., and S. M. Apte. 1992. Simulation of cell rolling and adhesion on surfaces in shear flow: general results and analysis of selectin-mediated neutrophil adhesion. *Biophys. J.* 63:35–37.

Israelachvili, J. N. 1985. Intramolecular and Surface Forces. Academic Press, New York.

Johnston, B., T. B. Issekutz, and P. Kubes. 1996. The alpha 4-integrin supports leukocyte rolling and adhesion in chronically inflamed postcapillary venules in vivo. *J. Exp. Med.* 183:1995–2006.

Ladd, A. C. J. 1994. Numerical simulations of particulate suspensions via a discretized Boltzmann equation. I. Theoretical foundation. *J. Fluid Mech.* 271:285–309.

Less, J. R., T. C. Skalak, E. M. Sevick, and R. K. Jain. 1991. Microvascular architecture in a mammary carcinoma: branching patterns and vessel dimensions. *Cancer Res.* 51:265–273.

Ley, K., T. F. Tedder, and G. S. Kansas. 1993. L-selectin can mediate leukocyte rolling in untreated mesenteric venules in vivo independent of E- or P-selectin. *Blood.* 82:1632–1638.

Mayrovitz, H. N., S. J. Kang, B. Herscovici, and R. N. Sampsell. 1987. Leukocyte adherence initiation in skeletal muscle capillaries and venules. *Microvasc. Res.* 33:22–34.

Melder, R. J., L. L. Munn, S. Yamada, C. Ohkubo, and R. K. Jain. 1995. Selectin- and integrin-mediated T-lymphocyte rolling and arrest on TNF-a-activated endothelium: augmentation by erythrocytes. *Biophys. J.* 69: 2131–2138.

Melder, R. J., J. Yuan, L. L. Munn, and R. K. Jain. 2000. Erythrocytes enhance lymphocyte rolling and arrest in vivo. *Microvasc. Res.* 59:316–322.

Migliorini, C., Y. Qian, H. Chen, E. Brown, R. Jain, and L. Munn. 2002. Red blood cells augment leukocyte rolling in a virtual blood vessel. *Biophys. J.* 83:1834–1841.

Munn, L. L., R. J. Melder, and R. K. Jain. 1996. Role of erythrocytes in leukocyte-endothelial interactions: mathematical model and experimental validation. *Biophys. J.* 71:466–478.

oude Egbrink, M. G., G. H. Janssen, K. Ookawa, D. W. Slaaf, R. S. Reneman, X. H. Wehrens, K. J. Maaijwee, N. Ohshima, H. A. Struijker Boudier, and G. J. Tangelder. 2002. Especially polymorphonuclear leukocytes, but also monomorphonuclear leukocytes, roll spontaneously in venules of intact rat skin: involvement of E-selectin. *J. Invest. Dermatol.* 118:323–326.

Pearson, M. J., and H. H. Lipowsky. 2000. Influence of erythrocyte aggregation on leukocyte margination in postcapillary venules of rat mesentery. *Am. J. Physiol. Heart Circ. Physiol.* 279:H1460–H1471.

Qian, Y. H., D. d'Humieres, and P. Lallemand. 1992. Lattice BGK models for Navier-Stokes equations. *Europhys. Lett.* 17:479–483.

Schmid-Schönbein, G. W., S. Usami, R. Skalak, and S. Chien. 1980. The interaction of leukocytes and erythrocytes in capillary and postcapillary vessels. *Microvasc. Res.* 19:45–70.

Skalak, R., and P.-I. Brånemark. 1969. Deformation of red blood cells in capillaries. *Science.* 164:717–719.

Skalak, R., and S. Chien. 1987. Handbook of Bioengineering. McGraw-Hill, New York.

Sun, C. H. 2000. Adaptive lattice Boltzmann model for compressible flows: viscous and conductive properties. *Phys. Rev. E.* 61:2645–2653.

Tsai, A. G., D. Nolte, K. Messmer, and M. Intaglietta. 1992. Effect of oxygen (perflubron emulsion) on leukocyte-endothelial interaction in postcapillary venules. *Biomater. Artif. Cells Immobilization Biotechnol.* 20:959–961.

Tsukada, K., E. Sekizuka, C. Oshio, and H. Minamitani. 2001. Direct measurement of erythrocyte deformability in *diabetes mellitus* with a transparent microchannel capillary model and high-speed video camera system. *Microvasc. Res.* 61:231–239.

Warnock, R. A., S. Askari, E. C. Butcher, and U. H. von Andrian. 1998. Molecular mechanisms of lymphocyte homing to peripheral lymph nodes. *J. Exp. Med.* 187:205–216.

Yuan, J., R. J. Melder, R. K. Jain, and L. L. Munn. 2001. A lateral view flow system for studies of cell adhesion and deformation under flow conditions. *Biotechniques.* 30:388–394.

Zao, Y., S. Chien, and S. Weinbaum. 2001. Dynamic contact forces on leukocyte microvilli and their penetration of the endothelial glycocalyx. *Biophys. J.* 80:1124–1140.